Synthesis and Characterization of Aluminosilicate Catalysts from Volcano Mud for Biofuel Production with Different Feedstocks

Hartati Hartati[1*], Qurrota A'yuni[1], Nita Safira Dewi[1], Putri Bintang Dea Firda[1], Adiba Naila Izzah[1], Didik Prasetyoko[2], Harmami Harmami[2], and Shahrul Nizam Ahmad[3]

[1]*Department of Chemistry, Faculty of Science and Technology, Universitas Airlangga, Campus C, UNAIR, Mulyorejo, Surabaya 60115, Indonesia*

[2]*Department of Chemistry, Faculty of Science and Data Analytics, Institut Teknologi Sepuluh Nopember, Surabaya 60111, Indonesia*

[3]*School of Chemistry and Environment, Faculty Sains Gunaan, Universiti Teknologi Mara, Selangor 40450, Malaysia*

Corresponding author:

email: hartati@fst.unair.ac.id

Received: May 14, 2024
Accepted: August 9, 2024

DOI: 10.22146/ijc.96149

Abstract: *The increasing awareness of sustainable development goals has led to the intensive development of biofuel as a substitute for fossil fuels. This study investigates the potency of volcano mud (VM) as the precursor in synthesizing aluminosilicate catalysts for biofuel production. Three catalysts were synthesized, A3, A3T, and A5, in a manner to investigate the effect of tetrapropylammonium hydroxide (TPAOH) addition and hydrothermal time on the crystallinity, Si/Al ratio, and textural properties of the catalysts. The catalytic activity of the synthesized catalysts was evaluated in two different qualities of feedstock, i.e., oleic acid (OA) and waste cooking oil (WCO). It is found that A5 which is synthesized with longer hydrothermal of 5 h has desirable properties, a high mesoporous surface area of 159 m^2/g, and a high acidity of 0.263 mmol/g. Catalyst A5 is proven to have similarly high catalytic activity in both WCO and OA feedstock, achieving a liquid yield of 93% with FAME selectivity of 95% for WCO and 95% liquid yield and FAME selectivity of 99% for OA feedstock. These results suggest that A5 is a versatile catalyst in biofuel production from either high or low-quality feedstocks.*

Keywords: *biofuel; aluminosilicate; oleic acid; waste cooking oil*

■ INTRODUCTION

Intensive exploration of fossil fuels has potentially led to the energy crisis. Moreover, fossil fuel combustion has caused a constant rise in CO_2 emissions. A study reported that 48% of the emitted anthropogenic CO_2 remains in the atmosphere, 26% is absorbed by the ocean, while the remaining 26% is absorbed by terrestrial ecosystems such as plants [1]. High concentration of CO_2 in the atmosphere potentially creates a greenhouse effect, which further leads to global warming, climate change, land weathering, etc. [2]. Moreover, the absorption of CO_2 by the surface of seawater leads to ocean acidification, which further triggers the calcification of reef organisms [3]. Therefore, the development of renewable energies is crucial to achieving the sustainable development goals (SDGs) of affordable and clean energy, climate action, and protecting life on land and below water.

Various renewable energies, such as solar panels, wind turbines, hydropower turbines, geothermal power, and biofuel [4], are intensively developed. Among them, biofuel is one versatile renewable energy because it has similar essential properties to fossil fuel, has cleaner combustion, is biodegradable, and can be used directly as the replacement for fossil fuel without significant modification in the engine or system [5]. Moreover, biofuel can be produced from various feedstocks, i.e., biomass, waste materials, and genetically modified organisms [6]. Accordingly, biofuel is widely adopted in both developing and industrialized countries. The remarkable development of biofuel technology is widely reported in terms of types: from bioethanol to green

diesel, in terms of phase, from liquid biofuel to gas and solid biofuel, and so forth [7]. Yet, biofuel development is continuing to date to satisfy the goal of affordable and accessible clean renewable energy.

In biofuel production, the type and quality of the feedstock are the main factors that strongly affect production efficiency. Generally, biofuel is produced from fatty acid esterification with short-chain alcohol like methanol [8]. Fatty acid feedstock can be obtained from chemical reagents but they lead to high production costs, especially in large-scale production. Another alternative is using oil as a fatty acid source in biofuel production, for example, palm oil [9] and castor oil [10]. The utilization of edible palm oil as feedstock in biofuel production creates competition with food sectors. In contrast, the use of non-edible castor presents the challenge of a time-consuming and expensive oil extraction process. One promising solution is using residue or waste products such as waste cooking oil. The use of waste products as feedstock in biofuel production implements the circular economic principle in addressing the SDGs of responsible consumption and production.

Aside from the feedstock, the type of catalyst also significantly affects the biofuel production efficiency. Catalysts facilitate a high reaction rate by decreasing the activation energy, leading to a high reaction yield [11]. In conventional industrial-scale biofuel production, basic homogeneous catalysts such as NaOH or KOH are widely used since they are low-cost and have high activity. However, the performance of basic catalysts is known to be severely decreased in low-quality feedstock with high FFA and water content due to saponification [12]. Additionally, homogeneous catalysts led to the tedious separation and neutralization process, producing toxic waste. On the contrary, heterogeneous acid catalysts have advantageous properties of being insensitive to saponification, easy separation, reusable, environmentally friendly, high activity, and selectivity [13]. Aluminosilicate is a potential heterogeneous catalyst with the unique characteristic of Brønsted and Lewis acidic sites: it has adjustable acidity, particle size, porosity, and high surface area [14].

Generally, aluminosilicate catalysts are synthesized from chemical precursors such as sodium aluminate, sodium silicate, and tetraethyl orthosilicate [15]. Natural materials like kaolin clays are also widely reported to be used as silica-alumina precursors in the synthesis of aluminosilicate catalysts [16]. However, kaolin clay mining has led to environmental problems such as water contamination, air pollution, and waste generation [17]. One potential material that can be used as a silica-alumina precursor is volcano mud (VM), which is obtained from mud eruption points, generally formed by geological activity below the Earth's surface. However, VM can also be triggered by drilling processes such as the one located in Sidoarjo, Indonesia, which is known as the Lapindo mud disaster. VM from Sidoarjo is reported to have high silica and sufficient alumina content [18]. In a previous study, zeolite Y was successfully synthesized from Lapindo mud [19]. Another study reported the utilization of Lapindo mud in the synthesis of zeolite and its application as an adsorbent [20]. The utilization of Lapindo mud as Ni catalyst support modified with amine group in hydrocracking of waste palm cooking oil was reported to yield 80 wt.% biofuel [21].

To date, the utilization of VM as a precursor in the synthesis of aluminosilicate catalysts and its application in biofuel production has not yet been reported. In this study, VM was used as a precursor for the synthesis of aluminosilicate catalysts for biofuel production. The use of VM as a silica-alumina precursor in the synthesis of aluminosilicate catalyst offers a cost-effective, environmentally favorable synthesis, also addressing the SDGs of responsible consumption and production and protecting life on land. The challenge arising from the utilization of natural material precursors is the high impurities content and low reactivity of the precursor [22]. Therefore, certain pre-treatment step is needed to remove impurities, extract, also activate the silica-alumina precursor. Herein, aluminosilicate catalysts were synthesized from VM extracted through a series of washing- acid leaching- and alkali treatment processes followed by a hydrothermal reaction. Further investigation was carried out to identify the relationship between the synthesis conditions i.e., TPAOH addition

and hydrothermal time, characteristic of the catalysts, and catalyst activity. The catalytic activity of aluminosilicate catalysts was evaluated in the biofuel production. Two different feedstocks were used, i.e. oleic acid and waste cooking oil as high- and low-quality feedstocks for biodiesel production, to investigate the effect of the quality of the feedstock on the catalysts' activity.

■ EXPERIMENTAL SECTION

Materials

VM (Lapindo mud) sample was taken from Sidoarjo, Indonesia. NaOH (99%, Merck), TPAOH (40 wt.%, Merck), silica colloidal (LUDOX 40 wt.%, Aldrich), ammonium acetate (CH_3COONH_4 98%, Merck), hydrochloric acid (HCl 37%, Merck), methanol (anhydrous, 99.8%, Aldrich), *n*-hexane (C_6H_{14}, ACS Reag., Merck), oleic acid ($C_{18}H_{34}O_2$, 65–88%, fluka), and deionized (DI) water were used as received. Waste cooking oil was obtained from household.

Instrumentation

The composition of the VM precursor was identified with an XRF spectrometer Philips Panalytical Minipal 4. XRD spectrometer Philips X-pert MPD-1 was used to identify the phase of the synthesized catalysts in the range 2θ of 5–50°. Chemical bonds and acidity tests of the catalysts were characterized with FTIR spectrometer Shimadzu IR Tracer-100 in the wavenumber range of 4000–400 cm^{-1}. The acidity test was carried out using pyridine as adsorbate. The morphology of the samples was observed using SEM (Carl Zeiss Evo EMA 10), and EDX was used to create map distribution and quantification of Si, O, and Al atoms. The porosity of the samples was analyzed by N_2 physisorption using Autosorb iQ Station 1 and evaluated by Brunauer-Emmet-Teller (BET) and Barrett-Joyner-Halenda (BJH) theories.

Procedure

Pre-treatment of VM

Prior to being used as a silica-alumina precursor in the aluminosilicate catalyst, VM was pre-treated through the washing, leaching, and extracting process. Initially, VM was washed with DI water, oven-dried at 100 °C overnight, and then sieved through 140 mesh sieves. The leaching process was performed by mixing pre-treated VM with HCl 1 M (1:5 w/v) and stirring for 2 h [23]. The mixture was then washed with DI water until pH neutral and the collected solid was oven-dried at 100 °C for 24 h, followed by calcination at 680 °C for 1 h. Afterward, the extraction of silica-alumina was done using the reflux method [24]. Calcined VM was mixed with NaOH 2 M (1:10) and then refluxed at 90 °C for 1 h. The silica-alumina content in the VM is extracted in the liquid phase [18].

Synthesis of catalysts

The aluminosilicate catalysts were synthesized by mixing 5.5 mL VM filtrate as a silica-alumina source, 11.0 mL LUDOX® as an additional silica source, and 60.0 mL DI water. The mixture was stirred continuously for 24 h for the aging process. A successful aging process was shown by the formation of colloidal gel [25]. The colloidal gel was then transferred to a Teflon-lined autoclave and heated in the oven at 190 °C for varied times (3 h and 5 h). After cooling down to room temperature, the mixture was then washed with DI water until pH neutral. The collected solid was then dried in the oven at 100 °C for 24 h. The catalyst synthesized through hydrothermal reaction for 3 h is annotated as A3 and A5 for the catalyst synthesized through 5 h hydrothermal reaction.

During hydrothermal, the aluminosilicate framework is formed through polycondensation between silica and alumina precursors. Conditions such as temperature and time play crucial roles in facilitating polycondensation [26]. Higher temperatures or longer hydrothermal time potentially led to the transformation of the amorphous aluminosilicate phase into a stable crystalline phase [27]. In this study, the investigation is focused on the effect of hydrothermal time on the characteristics of the synthesized catalyst. Therefore, the hydrothermal time is varied for 3 h and 5 h. The third sample was prepared using the same method as A3 but with the addition of 3 mL TPAOH, annotated as A3T. TPAOH is one crucial reagent that is widely used in the synthesizing zeolite with a high Si/Al mol ratio [28]. The quaternary ammonium ion of TPAOH helps maintain the stability of the aluminosilicate primary units that

have low alumina content [29]. In this study, TPAOH is used in the synthesis process to investigate how TPAOH affects the characteristics of the synthesized amorphous aluminosilicate.

Acidity test

The synthesized catalyst was oven-dried at 150 °C for 1 h to eliminate water and then molded and pressed into a pellet. The resulting pellet was placed in a nitrogen gas chamber, and then two drops of pyridine were dropped into the pellet and left for 1 h for the pyridine adsorption process. The pyridine desorption process was done by heat treatment in the furnace at 150 °C for 3 h. Afterward, the FTIR spectra were recorded. The peak areas at a wavelength of ~1540 and 1450 cm^{-1} were used to determine Lewis (L) and Brönsted (B) acid sites, respectively, according to the Eq. (1) [30]:

$$\text{Acidity}(\text{mmol}/\text{g}) = \frac{\text{B}\times\text{l}}{\text{K}\times\text{w}}\times 10^{-3} \quad (1)$$

where B is the peak area of B or L, w is sample mass (g), l is the area of the sample disk (cm^2) and k is the coefficient of acidity (L = 1.73 cm/μmol, B = 1.23 cm/ μmol, and B+L = 1.46 cm/μmol) [31].

Catalytic activity test

Since the catalysts were synthesized in the basic condition (NaOH), Na^+ is present in the aluminosilicate extra framework [32]. Before the evaluation of the catalytic performance, these Na^+ ions need to be cation exchanged with H^+ to form active acidic sites in the catalyst [33]. A mixture of 1 g catalyst and 25 mL ammonium acetate 0.5 M was refluxed at 60 °C for 3 h. Then, the mixture was filtered, and the collected catalyst was washed until it had a neutral pH. Afterwards, the catalyst was oven-dried at 100 °C for 24 h, followed by calcination at 550 °C for 6 h. During the process, Na^+ will be substituted with NH_4^+, producing sodium acetate, which will be removed during the washing process, whereas the ammonium will be removed during the calcination process, leaving an aluminosilicate catalyst with H^+ ions in the framework.

Before use, the cation-exchanged catalyst was thermally activated in the oven at 100 °C for 24 h. Then, 5 wt.% of the catalyst was mixed with 5 g of waste cooking oil and 20 mL methanol in the round bottom flask. The mixture refluxed at 65 °C with continuous stirring at 500 rpm for 2 h. After cooling down to room temperature, the mixture was then filtrated through filter paper, and the solid was collected as the spent catalyst. Then, the mixture was washed with *n*-hexane and oven-dried. The filtrate was mixed with 10 mL *n*-hexane in a separation funnel to extract the reaction product. To further identify the effect of feedstock quality, a catalytic activity test was carried out using oleic acid using a similar method referencing the reported study [34]. The liquid yield was calculated using the Eq. (2) [35].

$$\text{Liquid yield}\ (\%) = \left(\frac{\text{weight of liquid product}}{\text{weight of feedstock}}\right)\times 100\% \quad (2)$$

Analysis of liquid product from esterification

The GC-MS analysis was carried out using the Agilent 7890B instrument with parameters as follows: The temperature of the inlet was set to 200 °C, the injected sample was set to 1 μL with a split ratio of 10, a gradual increase of temperature was set to 60 °C initially, increased 10 °C/min to 150 °C, then increased further 5 °C/min to 250 °C. The column type used was HP-5MS with a 1 mL/min flow rate. The selectivity of the product was calculated using the Eq. (3) [36].

$$\text{Selectivity}(\%) = \left(\frac{\text{peak area of desired product}}{\text{peak area of total product}}\right)\times 100\% \quad (3)$$

■ RESULTS AND DISCUSSION

Effect of TPAOH and Hydrothermal Time on the Catalysts' Crystallinity

The diffractograms shown in Fig. 1(a) indicate that through the proposed synthesis method, the high crystalline peak of quartz (26.4°) content in the raw VM successfully transformed into amorphous aluminosilicate [22]. Broaden peak with a hump around 20–30° shown in sample A3 confirmed that the product is pure amorphous aluminosilicate. In comparison, sample A3T showed the initial growth of ZSM-5, indicated by the small peaks at 7.8°, 9.4°, and 25.6° (JCPDS No 43-0321). This result is consistent with a previous study which reported that utilization of TPAOH in aluminosilicate synthesis led to the formation of ZSM-5 [37]. TPA^+ induces the growth of MFI zeolite crystal through the formation of a clathrate structure between TPA^+ and

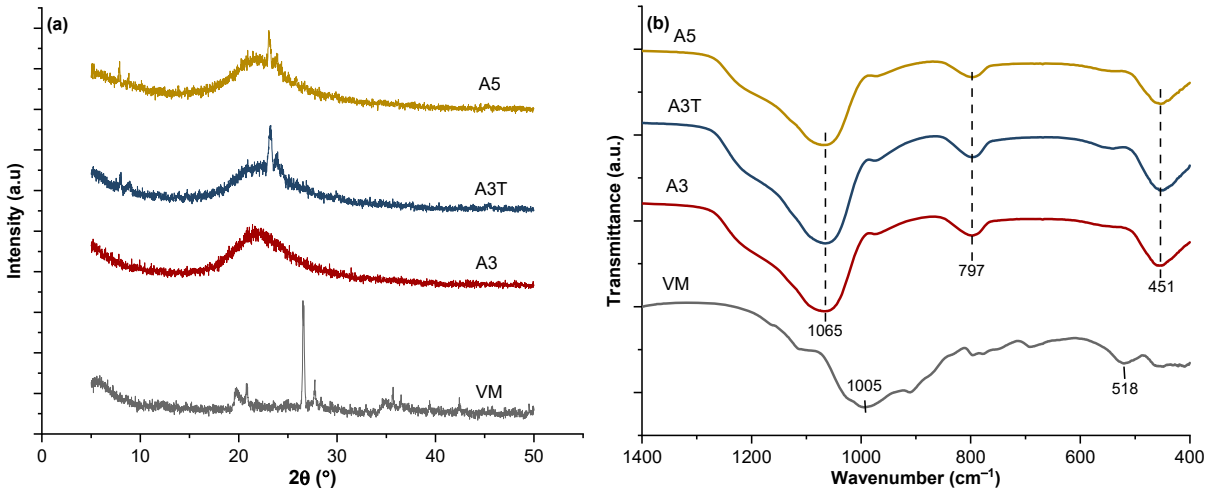

Fig 1. (a) X-ray diffractogram and (b) FTIR spectra of the VM precursor and the synthesized catalysts

water molecules in solution, which then isomorphously substituted by silicate and aluminate [38]. On the other hand, without the addition of TPAOH, sample A5 also showed a small characteristic peak of ZSM-5, which was induced by a prolonged reaction time of 5 h [39]. The calculated degree of crystallinity of samples A3T and A5 are 16.34 and 11.67%, respectively.

FTIR spectra of the synthesized catalyst are shown in Fig. 1(b). The VM showed adsorption bands at 1005, 798, and 518 cm^{-1}, which are attributed to the asymmetric stretching Si–O–Al, symmetric stretching Si–O–Al, and bending vibration of Si–O and Al–O, respectively [40]. The synthesized catalysts showed similar spectra with strong absorption bands at ~1065 cm^{-1} and small bands at ~797 cm^{-1}, ascribed to asymmetric and symmetric stretching of Si–O–Al, respectively [41]. Whereas small absorption at ~451 cm^{-1} is attributed to the bending vibration of Si–O and Al–O. Sample A3T and A5 showed distinct absorption bands of MFI structure at ~539 cm^{-1} and bending vibration of Si–OH at ~970 cm^{-1} [42].

Effect of TPAOH and Hydrothermal Time on the Si/Al Mole Ratio of the Catalysts

As depicted in Fig. 2, the morphology of the samples observed through SEM showed irregular particle chunks, which indicate the amorphous phase of the synthesized aluminosilicate. Fig. 3 shows the EDX mapping of the element in the synthesized catalysts. Higher hydrothermal time slightly increases the Si/Al mole ratio from 11 (A3) to 12.2 (A5), whereas the addition of TPAOH as structure structure-directing agent significantly increases the Si/Al mole ratio from 11 (A3) to 27 (A3T). A previous study reported that a high Si/Al mole ratio could be caused by the presence of TPA^+, which led to the formation of proximal framework Al atoms [38], resulting in the high Si content in the framework.

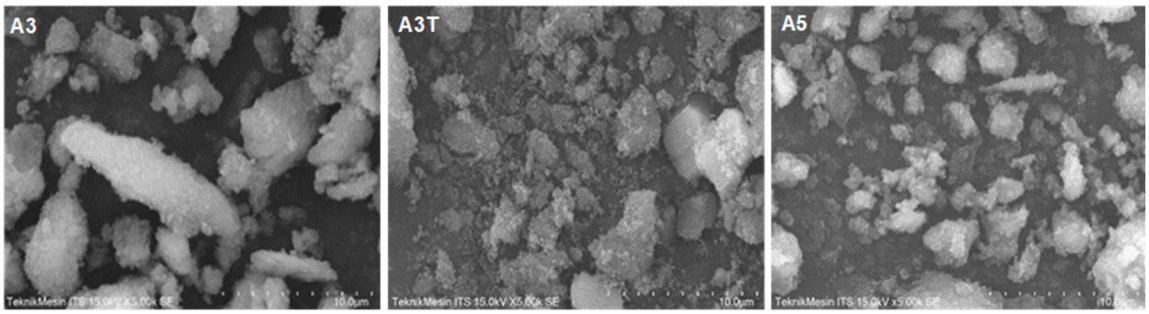

Fig 2. SEM images of the synthesized catalysts

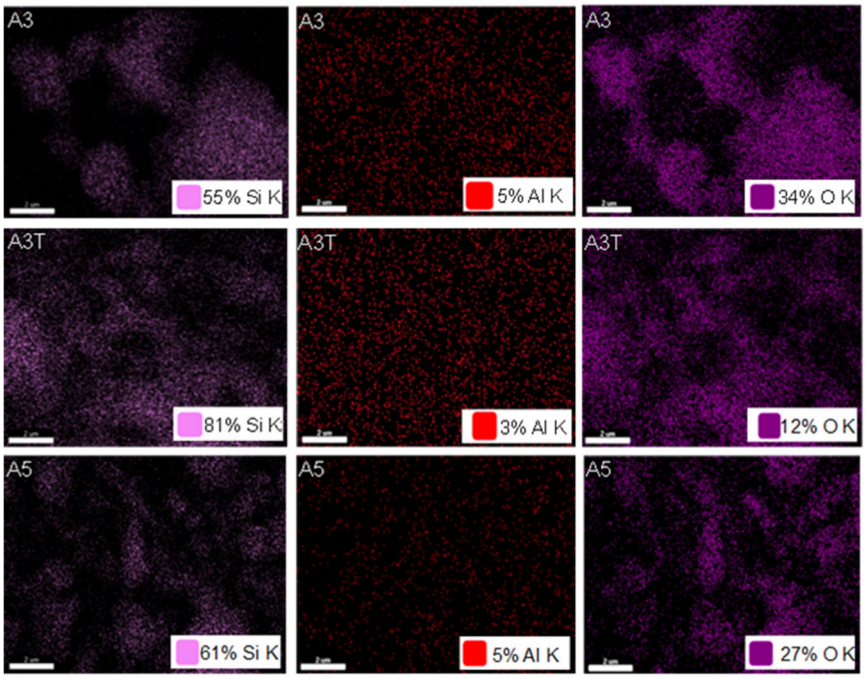

Fig 3. EDX elemental mapping of the synthesized catalysts. The white bar in the left corner of each picture represents the scale of 2 μm

Table 1. Textural properties of the synthesized catalysts

Code	Si/Al[a]	SA_{meso}[b] (m^2/g)	SA_{micro}[c] (m^2/g)	V_{pore} (cc/g)	d_{pore} (nm)	Acidity (mmol/g)		
						B	L	B+L
A3	11	114.000	85.800	1.080	31.400	0.052	0.022	0.074
A3T	27	147.400	128.000	1.270	31.200	0.002	0.106	0.108
A5	12	159.500	113.500	1.340	31.200	0.002	0.261	0.263

[a] = EDX; [b] = BJH; [c] = BET

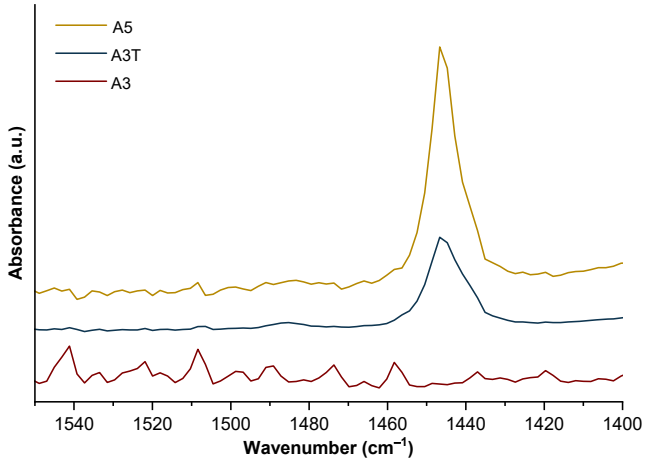

Fig 4. Pyridine FTIR spectra of synthesized catalysts

Acidity of the Catalysts

FTIR pyridine spectra of the synthesized catalysts are depicted in Fig. 4. High absorbance peak ~1440 cm^{-1} showed by sample A5 and A3T is attributed to the C–C stretching vibration of the pyridine that interacts with Lewis acidic sites [43]. Whereas the absorbance peak at ~1540 cm^{-1} shown by A3 is attributed to the C–C stretching vibration of pyridinium ions present in the Bronsted acid sites. As summarized in Table 1, sample A5 has the highest Lewis acidity of 0.261 mmol/g, whereas sample A3 has the highest Bronsted acidity configuration with a limited percentage of 0.052 mmol/g.

Effect of TPAOH and Hydrothermal Time on the Catalysts' Textural Properties

Nitrogen physisorption analysis was done to identify the porosity of the synthesized catalysts. The isotherm curves are depicted in Fig. 5(a). All samples

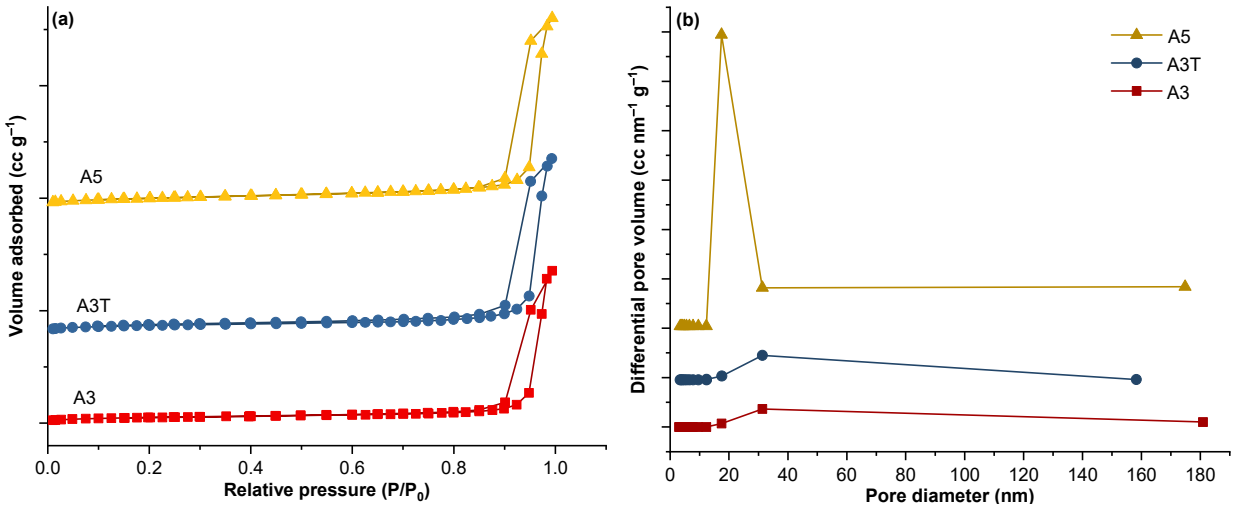

Fig 5. Isotherm graph of the (a) synthesized catalysts and (b) pore distribution of the synthesized catalysts determined from isotherm data

showed insignificant steep at low partial pressure ($p/p_0 < 0.01$), indicating the minority of micropores. The plateau with hysteresis was observed as the partial pressure increased to p/p_0 ~0.9, suggesting the formation of multilayer and capillary condensation in mesoporous and macroporous structures [44]. A significant increase in adsorption volume at p/p_0 close to 1 is characteristic of macropores between aluminosilicate catalysts aggregates [45]. The pore distribution graph of all catalysts in Fig. 5(b) confirms the presence of mesopores in the range of 15–32 nm and macropores in the range of 150–160 nm. Further analysis using BJH and BET methods is summarized in Table 1. All samples have similar average pore diameters of ~31 nm. Interestingly, it is found that the introduction of TPAOH significantly enhanced both microporous surface area from 85.8 (A3) to 128 m^2/g (A3T) and mesoporous surface area from ~114 (A3) to 147 m^2/g (A3T). However, sample A5 which was synthesized with a longer time, showed a slightly higher mesoporous area of ~159 m^2/g than sample A3T.

The Catalytic Activity of the Catalysts in Different Feedstock

Fig. 6 shows the liquid yield and product selectivity determined from GC-MS analysis. Using WCO feedstock, catalysts A3 and A3T obtained 67 and 81% liquid yields with FAME selectivity of 85 and 95%, respectively. Using the same catalysts in OA feedstock, a

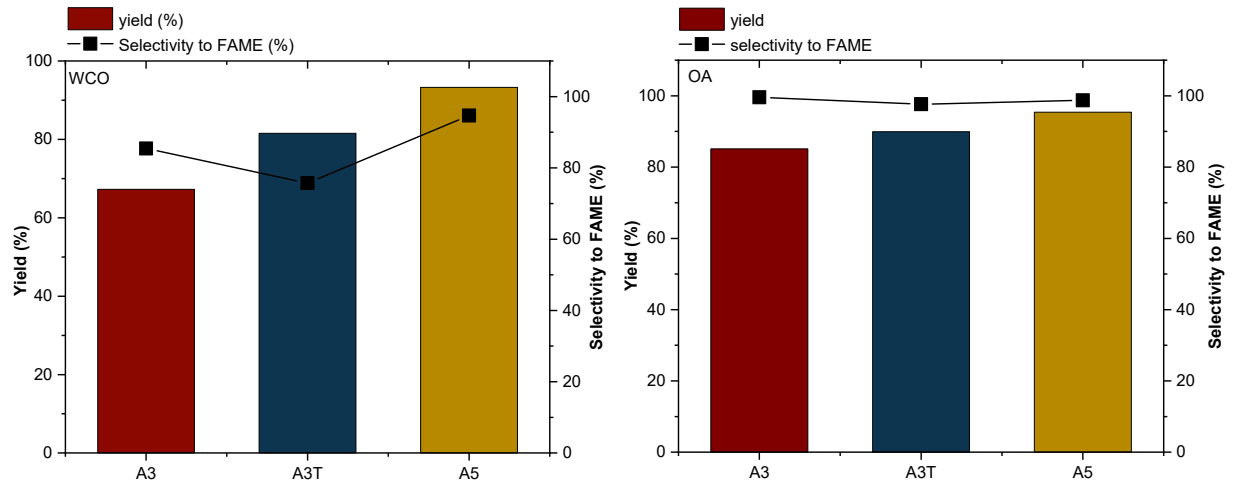

Fig 6. Yield and selectivity of FAME from WCO and OA feedstock with different catalysts

Table 2. Biofuel production from different catalysts and feedstocks

Feedstock type/ alcohol	Catalyst type	Temp (°C)	Time (h)	Yield (%)	Ref
WCO/MeOH (1/40)	Aluminosilicate (5.0 wt.%)	65	2.00	93.00	this work
Soybean oil/MeOH (1/30)	Aluminosilicate (14.0 wt.%)	130	12.00	41.00	[46]
OA/MeOH (1/40)	Aluminosilicate (5.0 wt.%)	65	2.00	95.00	this work
OA/MeOH (1/30)	Al-SBA-15 (10.0 wt.%)	150	2.00	75.00	[47]
Lauric acid/ MeOH (1/50)	Al-SBA-15 (5.0 wt.%)	65	2.00	79.00	[48]
WCO/MeOH (1/15)	Al-SBA-15 (1.0 wt.%)	200	0.50	71.96	[49]
WCO/MeOH (1/10)	Zeolite A (2.5 wt.%)	70	4.00	74.27	[50]

higher liquid yield of 85 and 90% was obtained for A3 and A3T, with FAME selectivity of 99 and 97%, respectively. Interestingly, catalyst A5 showed similarly high catalytic activity in both WCO and OA feedstock. Catalyst A5 obtained a high liquid yield of 93% with FAME selectivity of 95% when WCO was used as feedstock. In another study, a similar amorphous aluminosilicate catalyst was synthesized using aluminum acetylacetonate as the alumina source. The catalyst was reported to have 41% yield using soybean oil feedstock, 5 wt.% catalyst, under a significantly higher reaction temperature of 130 °C for 12 h [46]. Utilizing OA feedstock, catalyst A5 also showed a high performance of 95% liquid yield with FAME selectivity of 99%. Under a significantly higher reaction temperature of 150 °C for 2 h in OA feedstock, 10 wt.% of Al-SBA-15 catalyst showed a yield of 75% [47]. Under a similarly mild reaction condition of 65 °C for 2 h, using lauric acid feedstock with a slightly higher amount of methanol, 5 wt.% of catalyst Al-SBA-15 showed a yield of 79% [48]. The high catalytic activity of A5 in both WCO and OA feedstock is presumably due to the high mesoporous surface area and high acidity.

Table 2 shows the catalytic performance of different aluminosilicate-based catalysts in biofuel production. At a significantly higher reaction temperature of 200 °C for 30 min, 1 wt.% catalyst Al-SBA-15 has a yield of 71.96% for WCO feedstock [49]. Another study reported that using WCO feedstock, 2.5 wt.% zeolite A catalyst has a 74.27% yield at 70 °C for 4 h [50]. In our study, 5 wt.% of catalyst A5 showed a significantly higher yield of 93% under a relatively mild reaction temperature of 65 °C for 2 h with WCO feedstock. Table 2 shows that catalyst A5 is a promising and versatile catalyst for biodiesel production. The catalyst A5 showed high performance in low-quality WCO feedstock indicating its versatility.

■ CONCLUSION

Aluminosilicate catalysts were successfully synthesized from the extract of Lapindo mud. The variation of hydrothermal reaction time showed that a pure aluminosilicate catalyst was produced at a reaction time of 3 h (A3). Continuing the reaction to 5 h indicates the initial growth of the crystalline product (A5). It is found that the addition of TPAOH as a structure structure-directing agent in the optimum synthesis method of A3 promotes the growth of crystalline product (A3T) and increases the Si/Al ratio to 27. Desirable catalyst properties of a high mesoporous surface area of 159 m^2/g and high acidity of 0.263 mmol/g are shown by catalyst A5. Catalyst A5, which has the best catalyst properties, showed advantageous results of similarly high catalytic activity in both esterification of OA and WCO. In WCO feedstock, catalyst A5 obtained a high liquid yield of 93% with FAME selectivity of 95% was obtained. Meanwhile, in OA feedstock, catalyst A5 obtained a high liquid yield of 95% with FAME selectivity of 99%. A future study can be carried out by modification of the catalyst using metal as the dopant. Further investigation of the catalyst's activity and reusability is highly recommended to provide a more comprehensive future study.

■ ACKNOWLEDGMENTS

This work is supported by funding from DRPM Directory, Ministry of Research, Technology and Higher Education Indonesia, under the research project of *Penelitian Dasar* (PD) 2022, No: 770/UN3.15/PT/2022.

■ CONFLICT OF INTEREST

There are no conflicts to declare.

■ AUTHOR CONTRIBUTIONS

Hartati Hartati: conceptualization, supervision, validation, writing: review & editing; Qurota A'yuni: conceptualization; Nita Safira Dewi: formal analysis, data curation; Putri Bintang Dea Firda: visualization, writing-original draft; Adiba Naila Izzah: data curation, visualization; Didik Prasetyoko: writing: review & editing; Harmami: writing: review & editing; Shahrul Nizam Ahmad: writing: review & editing.

■ REFERENCES

[1] Friedlingstein, P., O'Sullivan, M., Jones, M.W., Andrew, R.M., Bakker, D.C.E., Hauck, J., Landschützer, P., Le Quéré, C., Luijkx, I.T., Peters, G.P., Peters, W., Pongratz, J., Schwingshackl, C., Sitch, S., Canadell, J.G., Ciais, P., Jackson, R.B., Alin, S.R., Anthoni, P., Barbero, L., Bates, N.R., Becker, M., Bellouin, N., Decharme, B., Bopp, L., Brasika, I.B.M., Cadule, P., Chamberlain, M.A., Chandra, N., Chau, T.T.T., Chevallier, F., Chini, L.P., Cronin, M., Dou, X., Enyo, K., Evans, W., Falk, S., Feely, R.A., Feng, L., Ford, D.J., Gasser, T., Ghattas, J., Gkritzalis, T., Grassi, G., Gregor, L., Gruber, N., Gürses, Ö., Harris, I., Hefner, M., Heinke, J., Houghton, R.A., Hurtt, G.C., Iida, Y., Ilyina, T., Jacobson, A.R., Jain, A., Jarníková, T., Jersild, A., Jiang, F., Jin, Z., Joos, F., Kato, E., Keeling, R.F., Kennedy, D., Klein Goldewijk, K., Knauer, J., Korsbakken, J.I., Körtzinger, A., Lan, X., Lefèvre, N., Li, H., Liu, J., Liu, Z., Ma, L., Marland, G., Mayot, N., McGuire, P.C., McKinley, G.A., Meyer, G., Morgan, E.J., Munro, D.R., Nakaoka, S.I., Niwa, Y., O'Brien, K.M., Olsen, A., Omar, A.M., Ono, T., Paulsen, M., Pierrot, D., Pocock, K., Poulter, B., Powis, C.M., Rehder, G., Resplandy, L., Robertson, E., Rödenbeck, C., Rosan, T.M., Schwinger, J., Séférian, R., Smallman, T.L., Smith, S.M., Sospedra-Alfonso, R., Sun, Q., Sutton, A.J., Sweeney, C., Takao, S., Tans, P.P., Tian, H., Tilbrook, B., Tsujino, H., Tubiello, F., van der Werf, G.R., van Ooijen, E., Wanninkhof, R., Watanabe, M., Wimart-Rousseau, C., Yang, D., Yang, X., Yuan, W., Yue, X., Zaehle, S., Zeng, J., and Zheng, B., 2023, Global carbon budget 2023, *Earth Syst. Sci. Data*, 15, 5301–5369.

[2] Panja, P., 2021, Deforestation, Carbon dioxide increase in the atmosphere and global warming: A modelling study, *Int. J. Modell. Simul.*, 41 (3), 209–219.

[3] Liang, Y., Xu, S., Zhu, M., Jiang, J., Zhang, J., Zhou, G., Hu, N., Chen, X., and Kita, H., 2023, Catalytic oxidation performance and ion-exchange of Ti-MWW zeolite membrane with dual organic template agents and potassium carbonate, *J. Catal.*, 417, 432–444.

[4] Østergaard, P.A., Duic, N., Noorollahi, Y., Mikulcic, H., and Kalogirou, S., 2020, Sustainable development using renewable energy technology, *Renewable Energy*, 146, 2430–2437.

[5] Fathima Anjila, P.K., Tharani, G.R., Sundaramoorthy, A., Kumar Shanmugam, V., Subramani, K., Chinnathambi, S., Pandian, G.N., Raghavan, V., Grace, A.N., Ganesan, S., and Rajendiran, M., 2024, An ultra-sensitive detection of melamine in milk using rare-earth doped graphene quantum dots- Synthesis and optical spectroscopic approach, *Microchem. J.*, 196, 109670.

[6] Panpatte, D.G., and Jhala, Y.K., 2019, "Agricultural Waste: A Suitable Source for Biofuel Production" in *Prospects of Renewable Bioprocessing in Future Energy Systems*, Eds. Rastegari, A.A., Yadav, A.N., and Gupta, A., Springer International Publishing, Cham, Switzerland, 337–357.

[7] Mat Aron, N.S., Khoo, K.S., Chew, K.W., Show, P.L., Chen, W.H., and Nguyen, T.H.P., 2020, Sustainability of the four generations of biofuels – A review, *Int. J. Energy Res.*, 44 (12), 9266–9282.

[8] Prates, C.D., Ballotin, F.C., Limborço, H., Ardisson, J.D., Lago, R.M., and Teixeira, A.P.D.C., 2020, Heterogeneous acid catalyst based on sulfated iron ore tailings for oleic acid esterification, *Appl. Catal., A*, 600, 117624.

[9] Dey, S., Reang, N.M., Das, P.K., and Deb, M., 2021, A comprehensive study on prospects of economy,

environment, and efficiency of palm oil biodiesel as a renewable fuel, *J. Cleaner Prod.*, 286, 124981.

[10] Wu, Q., Shu, Q., Guo, W., and Xing, X., 2024, Preparation of Brönsted-Lewis dual acidic catalyst Ce-HPW-F and its simultaneous catalytic esterification and transesterification of oleic acid and castor oil with methanol to synthesize biodiesel, *Fuel*, 361, 130668.

[11] Nisar, J., Nasir, U., Ali, G., Shah, A., Farooqi, Z.H., Iqbal, M., and Shah, M.R., 2021, Kinetics of pyrolysis of sugarcane bagasse: Effect of catalyst on activation energy and yield of pyrolysis products, *Cellulose*, 28 (12), 7593–7607.

[12] Chanakaewsomboon, I., Tongurai, C., Photaworn, S., Kungsanant, S., and Nikhom, R., 2020, Investigation of saponification mechanisms in biodiesel production: Microscopic visualization of the effects of FFA, water and the amount of alkaline catalyst, *J. Environ. Chem. Eng.*, 8 (2), 103538.

[13] Ye, H., Shi, J., Wu, Y., Yuan, Y., Gan, L., Wu, Y., Xie, H., Pugazhendhi, A., and Xia, C., 2024, Research progress of nano-catalysts in the catalytic conversion of biomass to biofuels: Synthesis and application, *Fuel*, 356, 129594.

[14] Sánchez-Velandia, J.E., Gelves, J.F., Dorkis, L., Márquez, M.A., and Villa, A.L., 2019, Ring-opening of β-pinene epoxide into high-added value products over Colombian natural zeolite, *Microporous Mesoporous Mater.*, 287, 114–123.

[15] Vassilina, G., Umbetkaliyeva, K., Abdrassilova, A., Vassilina, T., and Zakirov, Z., 2022, The mesoporous aluminosilicate application as support for bifunctional catalysts for *n*-hexadecane hydroconversion, *Open Chem.*, 20 (1), 225–236.

[16] Feng, M., Kou, Z., Tang, C., Shi, Z., Tong, Y., and Zhang, K., 2023, Recent progress in synthesis of zeolite from natural clay, *Appl. Clay Sci.*, 243, 107087.

[17] Lapčík, V., Kohut, O., Novák, P., and Kaločajová, A., 2018, Environmental impacts of mining of mineral resources, *Inz. Miner.*, 2 (42), 253–263.

[18] A'yuni, Q., Rahmayanti, A., Hartati, H., Purkan, P., Subagyo, R., Rohmah, N., Itsnaini, L.R., and Fitri, M.A., 2023, Synthesis and characterization of silica gel from Lapindo volcanic mud with ethanol as a cosolvent for desiccant applications, *RSC Adv.*, 13 (4), 2692–2699.

[19] Andarini, N., Haryati, T., Suwardiyanto, S., and Sulistiyo, Y.A., 2022, Synthesis of zeolite Y from Lapindo mud with the comparative variation of the weight of NaOH/mud and molar SiO_2/Al_2O_3, *Indones. Chim. Lett.*, 1 (1), 8–12.

[20] Trimayanto, S., Aminudin, M.R., and Hertiwi, L.R., 2019, Synthesis of zeolite from Lapindo mud using the hydrothermal method as a lead heavy metal (Pb) adsorbent in industrial waste, *1st GCC International Conference on Industrial Engineering and Operations Management*, Riyadh, Saudi Arabia, 26–28 November 2019, 766–771.

[21] Trisunaryanti, W., Azizah, S.N., Fatmawati, D.A., Triyono, T., and Ningrum, N.C., 2022, Performance of a hybrid catalyst from amine groups and nickel nanoparticles immobilized on Lapindo mud in selective production of bio-hydrocarbons, *Indones. J. Chem.*, 22 (4), 896–912.

[22] Hartati, H., Prasetyoko, D., Santoso, M., Qoniah, I., Leaw, W.L., Firda, P.B.D., and Nur, H., 2020, A review on synthesis of kaolin-based zeolite and the effect of impurities, *J. Chin. Chem. Soc.*, 67 (6), 911–936.

[23] Zulfiqar, U., Subhani, T., and Husain, S.W., 2016, Synthesis and characterization of silica nanoparticles from clay, *J. Asian Ceram. Soc.*, 4 (1), 91–96.

[24] Li, X., Han, S., Guan, D., Jiang, N., Xu, J., and Park, S.E., 2021, Rapid direct synthesis of nano-H-ZSM-5 from leached illite via solid-like-state conversion-based crystallization, *Appl. Clay Sci.*, 203, 106028.

[25] Dapremont, A.M., and Wray, J.J., 2021, Insights into Mars mud volcanism using visible and near-infrared spectroscopy, *Icarus*, 359, 114299.

[26] Grand, J., Awala, H., and Mintova, S., 2016, Mechanism of zeolites crystal growth: New findings and open questions, *CrystEngComm*, 18 (5), 650–664.

[27] Okada, Y., Sada, Y., Miyagi, S., Yamada, H., Ohara, K., Yanaba, Y., Yoshioka, M., Ishikawa, T., Naraki,

Y., Sano, T., Okubo, T., Simancas, R., and Wakihara, T., 2025, Unraveling the relationship between aging conditions, properties of amorphous precursors and CHA-type zeolite crystallization, *Microporous Mesoporous Mater.*, 381, 113099.

[28] Tang, S., Zhang, C., Xue, X., Pan, Z., Wang, D., and Zhang, R., 2019, Catalytic pyrolysis of lignin over hierarchical HZSM-5 zeolites prepared by post-treatment with alkaline solutions, *J. Anal. Appl. Pyrolysis*, 137, 86–95.

[29] Asgar Pour, Z., and Sebakhy, K.O., 2022, A review on the effects of organic structure-directing agents on the hydrothermal synthesis and physicochemical properties of zeolites, *Chemistry*, 4 (2), 431–446.

[30] Emeis, C.A., 1993, Determination of integrated molar extinction coefficients for infrared absorption bands of pyridine adsorbed on solid acid catalysts, *J. Catal.*, 141 (2), 347–354.

[31] Wu, W., and Weitz, E., 2014, Modification of acid sites in ZSM-5 by ion-exchange: An *in-situ* FTIR study, *Appl. Surf. Sci.*, 316, 405–415.

[32] Alzeer, M.I.M., and MacKenzie, K.J.D., 2018, Synthesis and catalytic properties of new sustainable aluminosilicate heterogeneous catalysts derived from fly ash, *ACS Sustainable Chem. Eng.*, 6 (4), 5273–5282.

[33] Lanzafame, P., Barbera, K., Papanikolaou, G., Perathoner, S., Centi, G., Migliori, M., Catizzone, E., and Giordano, G., 2018, Comparison of H^+ and NH_4^+ forms of zeolites as acid catalysts for HMF etherification, *Catal. Today*, 304, 97–102.

[34] Hussein, M.F., Abo El Naga, A.O., El Saied, M., AbuBaker, M.M., Shaban, S.A., and El Kady, F.Y., 2021, Potato peel waste-derived carbon-based solid acid for the esterification of oleic acid to biodiesel, *Environ. Technol. Innovation*, 21, 101355.

[35] Yadav, N., Yadav, G., and Ahmaruzzaman, M., 2023, Fabrication of surface-modified dual waste-derived biochar for biodiesel production by microwave-assisted esterification of oleic acid: Optimization, kinetics, and mechanistic studies, *Renewable Energy*, 218, 119308.

[36] Trisunaryanti, W., Triyono, T., Paramesti, C., Larasati, S., Santoso, N.R., and Fatmawati, D.A., 2020, Synthesis and characterization of Ni-NH_2/mesoporous silica catalyst from Lapindo mud for hydrocracking of waste cooking oil into biofuel, *Rasayan J. Chem.*, 13 (3), 1386–1393.

[37] Nugraha, R.E., Prasetyoko, D., Asikin-Mijan, N., Bahruji, H., Suprapto, S., Taufiq-Yap, Y.H., and Jalil, A.A., 2021, The effect of structure directing agents on micro/mesopore structures of aluminosilicates from Indonesian kaolin as deoxygenation catalysts, *Microporous Mesoporous Mater.*, 315, 110917.

[38] Hur, Y.G., Kester, P.M., Nimlos, C.T., Cho, Y.R., Miller, J.T., and Gounder, R., 2019, Influence of tetrapropylammonium and ethylenediamine structure-directing agents on the framework Al distribution in B-Al-MFI zeolites, *Ind. Eng. Chem. Res.*, 58 (27), 11849–11860.

[39] Ryu, G.U., Kim, G.M., Khalid, H.R., and Lee, H.K., 2019, The effects of temperature on the hydrothermal synthesis of hydroxyapatite-zeolite using blast furnace slag, *Materials*, 12 (13), 2131.

[40] Ellerbrock, R., Stein, M., and Schaller, J., 2022, Comparing amorphous silica, short-range-ordered silicates and silicic acid species by FTIR, *Sci. Rep.*, 12 (1), 11708.

[41] Diwakar, J., Viswanadham, N., Saxena, S.K., Kumar, S., and Al-Muhtaseb, A.H., 2018, Liquid-phase solvent-less reactions for value addition of glycerol and phenols over nano porous aluminosilicates, *Mater. Today Commun.*, 15, 260–268.

[42] Maziz, A., Chouat, N., Bensafi, B., and Djafri, F., 2023, dTG and FTIR investigation of methanol behavior adsorbed within MFI-type zeolites, *J. Porous Mater.*, 30 (4), 1403–1415.

[43] Hartanto, D., Yuan, L.S., Mutia Sari, S., Sugiarso, D., Kris Murwarni, I., Ersam, T., Prasetyoko, D., and Nur, H., 2016, The use of the combination of FTIR, pyridine adsorption, ^{27}Al and ^{29}Si MAS NMR to determine the Brönsted and Lewis acidic sites, *J. Teknol.*, 78 (6), 223–228.

[44] Ramesh, K., Reddy, K.S., Rashmi, I., and Biswas, A.K., 2014, Porosity distribution, surface area, and morphology of synthetic potassium zeolites: A SEM and N_2 adsorption study, *Commun. Soil Sci. Plant Anal.*, 45 (16), 2171–2181.

[45] Soboleva, T., Zhao, X., Malek, K., Xie, Z., Navessin, T., and Holdcroft, S., 2010, On the micro-, meso-, and macroporous structures of polymer electrolyte membrane fuel cell catalyst layers, *ACS Appl. Mater. Interfaces*, 2 (2), 375–384.

[46] Xie, W., Wang, Q., Guo, L., and Zhang, Q., 2024, Improved biodiesel production from soybean oil using molybdenum-zirconium doped aluminosilicates as heterogeneous catalysts, *Bioenergy Res.*, 17 (1), 532–546.

[47] Canhaci, S.J., Albuquerque, E.M., Lopes, C.C., Faria, V.W., Chinelatto Junior, L.S., Duarte de Farias, A.M., Quitete, C.B., and Fraga, M.A., 2023, Balance between catalyst acidity and hydrophilicity in biofuel production from fatty acid esterification over Al-SBA-15, *Catalysts*, 13 (5), 827.

[48] Sahel, F., Sebih, F., Bellahouel, S., Bengueddach, A., and Hamacha, R., 2020, Synthesis and characterization of highly ordered mesoporous nanomaterials Al-MCM-41 and Al-SBA-15 from bentonite as efficient catalysts for the production of biodiesel MELA and EELA, *Res. Chem. Intermed.*, 46 (1), 133–148.

[49] Hossain, M.N., Siddik Bhuyan, M.S.U., Md Ashraful Alam, A.H., and Seo, Y.C., 2019, Optimization of biodiesel production from waste cooking oil using S–TiO_2/SBA-15 heterogeneous acid catalyst, *Catalysts*, 9 (1), 67.

[50] Derbe, T., Zereffa, E.A., Sani, T., and Girma, T., 2024, Synthesis of green heterogeneous bifunctional zeolite-A/biochar catalyst for the production of biodiesel from waste cooking oil, *Catal. Lett.*, 154 (10), 5530–5545.